



Iron/silicon carbide composites with tunable high-frequency magnetic and dielectric properties for potential electromagnetic wave absorption

Tong Gao^{1,2} · Huawei Rong² · Khaled H. Mahmoud³ · Jiachang Ruan¹ · Salah M. El-Bahy⁴ · Abeer A. Faheim⁵ · Yixing Li¹ · Mina Huang⁶ · Mohamed A. Nassan⁷ · Rongzhi Zhao^{1,2}

Received: 20 April 2022 / Revised: 13 May 2022 / Accepted: 24 May 2022 / Published online: 9 June 2022

© The Author(s), under exclusive licence to Springer Nature Switzerland AG 2022

Abstract

High-performance microwave absorption materials are desired to solve the electromagnetic interference and pollution problems. It has been recognized that the microwave absorption properties are highly correlated to the complex permittivity, the complex permeability, and their impedance matching, which could be achieved by composing dielectric and magnetic loss materials together. Here, we synthesized the core/shell structural Fe/SiC composites with tunable Fe/SiC ratios by a heat-assisted surface adhesion process. As a result, the mostly optimized absorbers could achieve the minimum reflection loss of -51 dB at the absorber thickness of 2.01 mm and the efficient absorption bandwidth (< -10 dB) is broadened to 7.6 GHz at the K-band (18–26.5 GHz). The present work provides a cost-effective strategy for synthesizing the Fe/SiC composites for microwave absorption applications.

Keywords Fe · SiC · Core/Shell · Interfacial polarization · Microwave absorption

1 Introduction

The microwave absorption materials have been widely investigated to solve the electromagnetic interferences and pollution caused by the integration and microminiaturization of electron devices [1–5]. To increase the microwave absorption properties at gigahertz, the effective combination between the dielectric and the magnetic loss of the absorber has attracted more attention [6–8]. Here, the dielectric and magnetic loss abilities, which are mainly associated with the complex permittivity ($\epsilon = \epsilon' + i\epsilon''$) and permeability ($\mu = \mu' + i\mu''$), have been achieved by the combination between carbon-based materials and ferromagnetic materials [9–12], such as FeCo/carbon [12–14], metal/carbon [15–20], Fe₃O₄/carbon [21–25], and metal/oxide [26–29]. However, the complex and expensive synthesis approaches of the aforementioned materials could thus limit their applications.

Consequently, microscale magnetic iron powders can be regarded as promising absorbers because of their high magnetic permeability and saturation magnetization. However, the deficiency of dielectric loss mechanism could thus result in the mismatch of electromagnetic impedance and reduce their loss abilities at gigahertz [30–35]. To solve these holdbacks and achieve a proper impedance matching, the efficient approach is to composite

✉ Huawei Rong
hwrong@hdu.edu.cn

¹ Key Laboratory for Anisotropy and Texture of Materials (MOE), School of Materials Science and Engineering, Northeastern University, Shenyang 110819, China

² Institute of Advanced Magnetic Materials, College of Materials and Environmental Engineering, Hangzhou Dianzi University, Hangzhou 310012, China

³ Department of Physics, College of Khurma University College, Taif University, P.O. Box 11099, Taif 21944, Saudi Arabia

⁴ Department of Chemistry, Turabah University College, Taif University, P.O. Box 11099, Taif 21944, Saudi Arabia

⁵ Department of Chemistry, Faculty of Science, Al-Azhar University, Nasr City, Cairo, Egypt

⁶ College of Materials Science and Engineering, Taiyuan University of Science and Technology, Taiyuan 030024, China

⁷ Department of Clinical Laboratory Sciences, Turabah University College, Taif University, P.O. Box 11099, Taif 21944, Saudi Arabia

them with other type absorbers, in which their absorption bandwidth and attenuation coefficient could be further optimized [35–37], for example, Fe/SiO₂ [38], Fe/TiO₂ [39], Fe/MnO₂ [40], Fe/CNT [41], and Fe/SiC [42]. Among all these candidates, silicon carbide (SiC) has received more concentrations ascribed to its excellent chemical stability, dielectric loss capability, and microwave absorption efficiency [43, 44]. It has been reported that the composites prepared through Fe and SiC could achieve satisfactory microwave absorption performances at gigahertz regions [45–47], in which the magnetic elements introduced magnetic loss abilities while the introduction of SiC tailors the impedance matching and meanwhile increases the dielectric loss performance. Despite these achievements, the SiC/Fe composites were usually fabricated by the mechanical milling process, which still requires a long preparation time and high energy cost. Thus, a simple synthesis approach to such core/shell structural composites needs to be explored.

In this work, we papered a series of core/shell structural Fe/SiC composites by a heat-assisted surface adhesion process. Their magnetic/dielectric impedance matching performance could be optimized by the synergistic effect of heterogeneous components. By adjusting the ratio of Fe and SiC powders, the electromagnetic properties could be tuned, resulting in a broad absorption bandwidth, strong reflection loss, and high microwave attenuation performance. Additionally, ascribing to the cost-effective production approach of Fe/SiC composites, it promises great potential in engineering applications. In addition, the applications of these composites can be evaluated in the thermoplastics and thermosetting systems with other functions to figure out their electromagnetic wave absorption performances [48–51].

2 Experimental

2.1 Preparation

Commercial iron powders (~35 μm) and silicon carbide powders (~500 nm) were purchased from ZhongNuo Advanced Material Technology Co., Ltd., Beijing, China. Firstly, iron powders and silicon carbide powders with a molar mass ratio of 2:1 were poured into a three-necked flask. Secondly, the mixture was annealed for 2 h at 120 °C with a stirring speed of 500 rpm under a nitrogen atmosphere. Finally, the as-made composite denoted as Fe:SiC 2:1 could be collected for usage. Fe:SiC 1:1, Fe:SiC 1:2, and Fe:SiC 1:3 composites were obtained by adjusting the molar mass ratio of two powders as 1:1, 1:2, and 1:3, respectively.

2.2 Characterizations

The phase component analysis was performed by X-ray diffraction (XRD) with a Cu-K α ($\lambda=0.15405$ nm) irradiation at

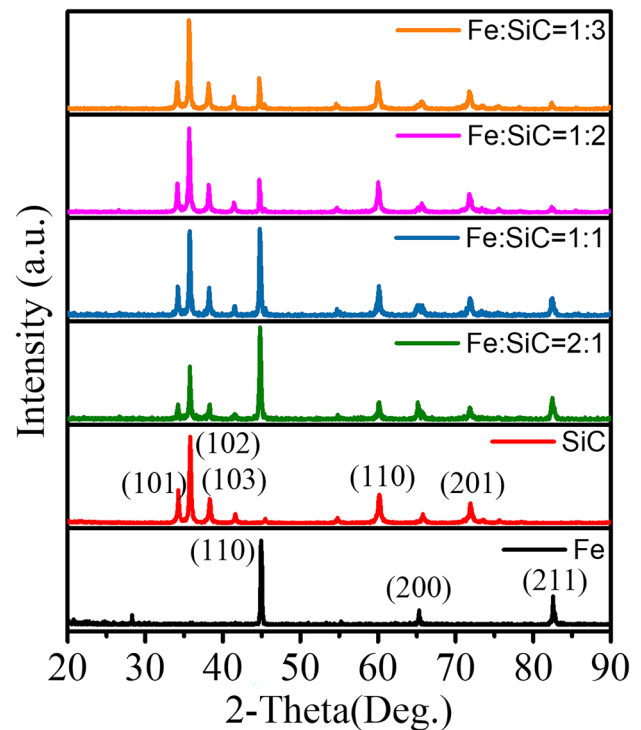


Fig. 1 The XRD patterns of Fe, SiC, and Fe/SiC composites

a voltage of 30 kV and a current of 30 mA at a scan step of 0.2°. The microstructure images were obtained by JEOL JSM-7001F field emission scanning electron microscope (FESEM) at an accelerating voltage of 15 kV. The magnetic hysteresis loop measurement was recorded on a Lakeshore vibrating sample magnetometer (VSM) with a magnetic field of ± 12 kOe.

2.3 Electromagnetic measurements

For measurement of the electromagnetic parameters, a Keysight N5222A vector network analyzer (VNA) was calibrated by the through-reflect-line (TRL) standard technique. The scattering parameters were tested by a K-band waveguide (Model: 42 WAL-100, A-INFOMW). The sample was produced by uniformly mixing the Fe/SiC composites with 30 wt% paraffin, in which the filling ratio is set as the maximum loading contents of the composited materials.

3 Results and discussion

The phase components were analyzed by XRD. Figure 1 shows the XRD patterns of the original Fe powders, SiC powders, and Fe/SiC composites synthesized at ratios of Fe to SiC of 2:1, 1:1, 1:2, and 1:3. The diffraction peaks at 44.7°, 65.0°, and 82.3° are aligned with the (110), (200), and (211) planes of the iron with body-centered

cubic (BCC) structure (JCPDS Card 65–4899). After surface modification, five new peaks appear at 34.2° , 35.8° , 38.2° , 60.2° , and 71.0° , respectively, which can be assigned to the (101), (102), (103), (110), and (201) planes of β -SiC (JCPDS Card 73–1663). It should be noted that the Fe peaks remain intact after SiC coating without the formation of other peaks, indicating the high degree of purity of the Fe/SiC composites. As the contents of SiC are increased, its diffraction peaks become more distinct, suggesting the increased coverages of SiC on the surface of Fe powders.

Morphologies of the synthesized products are presented in Fig. 2. SEM images (Fig. 2a) of the initial Fe powders indicate spherical shapes with a diameter of 30–40 μm . Figure 2b exhibits SiC powders of a flaky shape with a diameter of 500 nm. After the heat-assisted surface adhesion process of 2 h, the microstructures of Fe/SiC composites are shown in Fig. 2c, d, and e. Compared with Fig. 2a, it is clearly observed that the surface of the particles is not smooth, evidencing that the SiC powders are completely coated on the surface of Fe powders. This is further affirmed by energy-dispersive spectrometer (EDS) results, illustrating the Si and Fe elemental distribution

for an individual core/shell structural particle, as shown in Fig. 2f, g.

Field-dependent magnetization curves and the diagram of saturation magnetization and coercivity of Fe and Fe/SiC composites with different ratios are presented in Fig. 3a, b. The magnetic hysteresis loops were measured at room temperature between the magnetic field range of ± 12 kOe. The Fe and Fe/SiC powders with ratios of 2:1, 1:1, 1:2, and 1:3 are corresponding to the saturation magnetizations (M_s) of 193 emu/g, 161 emu/g, 127 emu/g, 92 emu/g, and 67 emu/g, the coercive fields (H_c) of 26.2 Oe, 13.5 Oe, 11.7 Oe, 10.8 Oe, and 20.5 Oe, respectively. They all have a declining trend due to the increase of the non-magnetic SiC components. The residual magnetization of all the samples was low, indicating that the Fe/SiC composites were soft magnetic at room temperature. Figure 3b shows that the saturation magnetization and coercivity are gradually decreased along with the ratio of SiC powders increasing. The increasing SiC contents could accelerate the formation of SiC shells on the Fe powders; such additional non-magnetic materials could thus reduce the M_s values.

The relatively complex permeability ($\mu_r = \mu' - j\mu''$) and the relatively complex permittivity ($\epsilon_r = \epsilon' - j\epsilon''$) were

Fig. 2 The SEM images and elemental mapping of samples. **a** Fe powders, **b** SiC powders, **c–f** Fe:SiC 1:3 composite with different magnifications, and **g** the Fe and Si element overlay mapping images

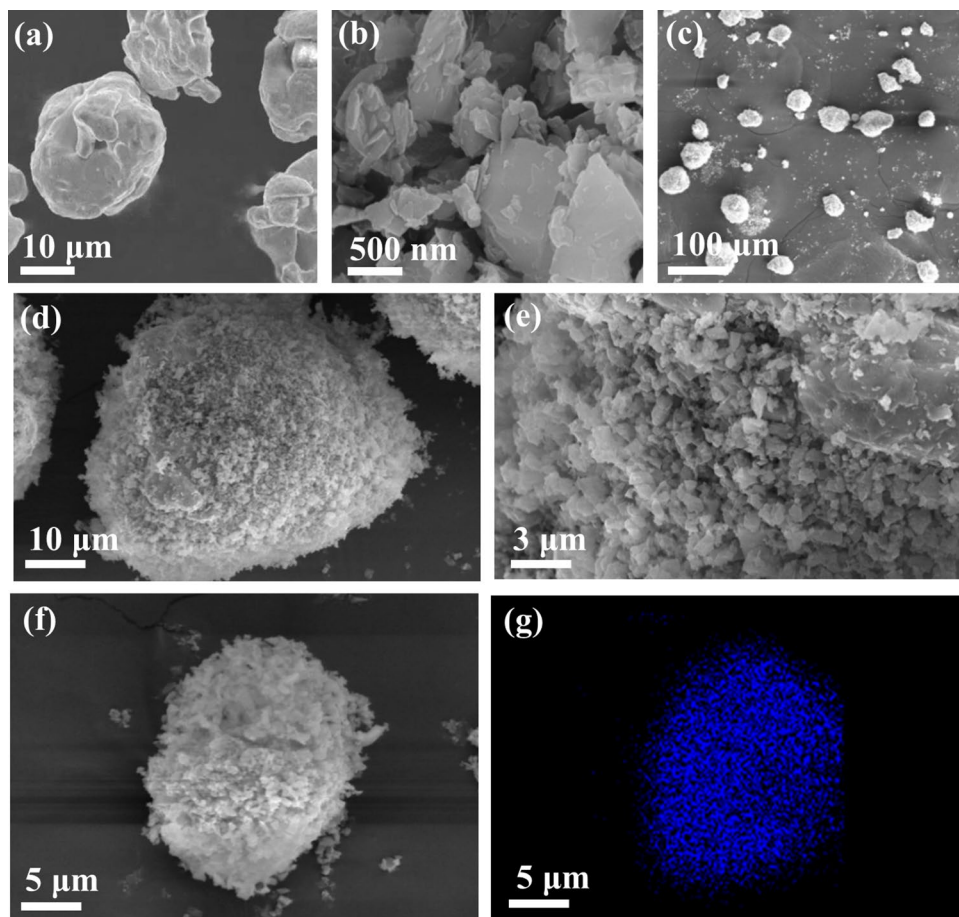
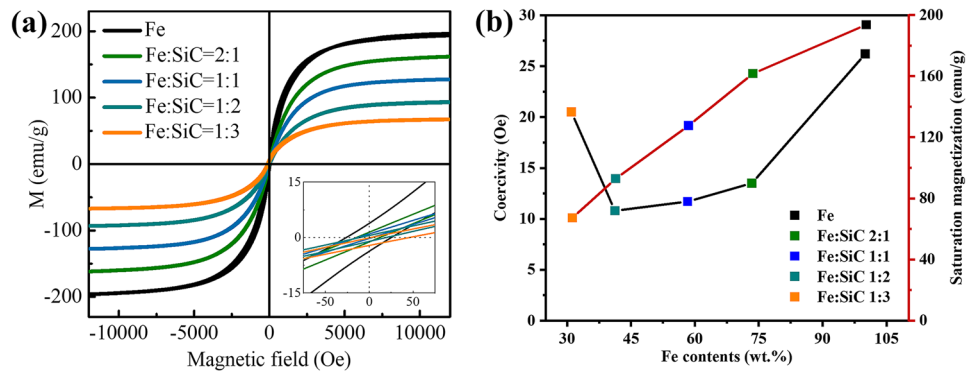


Fig. 3 Magnetic performances. **a** The magnetic hysteresis loops of Fe and Fe/SiC composites with different ratios. **b** The diagram of saturation magnetization and coercivity as a function of ratios



measured at the frequency range of 18–26.5 GHz (K-band). Figure 4a, b show the real part (μ') and imaginary part (μ'') of complex permeability (μ_r) of Fe and Fe/SiC composites with different ratios. The μ' of almost all the coated samples are higher than the original Fe powders. The μ'' of Fe/SiC composites at ratios of 1:1 and 1:3 are lower than Fe powders, while the others show opposite changes. The tangential magnetic loss ($\tan\delta_m = \mu''/\mu'$) and the tangential dielectric

loss ($\tan\delta_e = \epsilon''/\epsilon'$) had a dominant influence on the EM absorption [52]. The frequency-dependent tangential magnetic loss of Fe/SiC composites is presented in Fig. 4c. The $\tan\delta_m$ values of all powders are quite low, within the range of 0 to 0.2. The decreasing trend of $\tan\delta_m$ versus frequency was almost the same for all samples, and meanwhile the magnetic loss capability has been decreased due to the corresponding increase of the SiC nanoparticles.

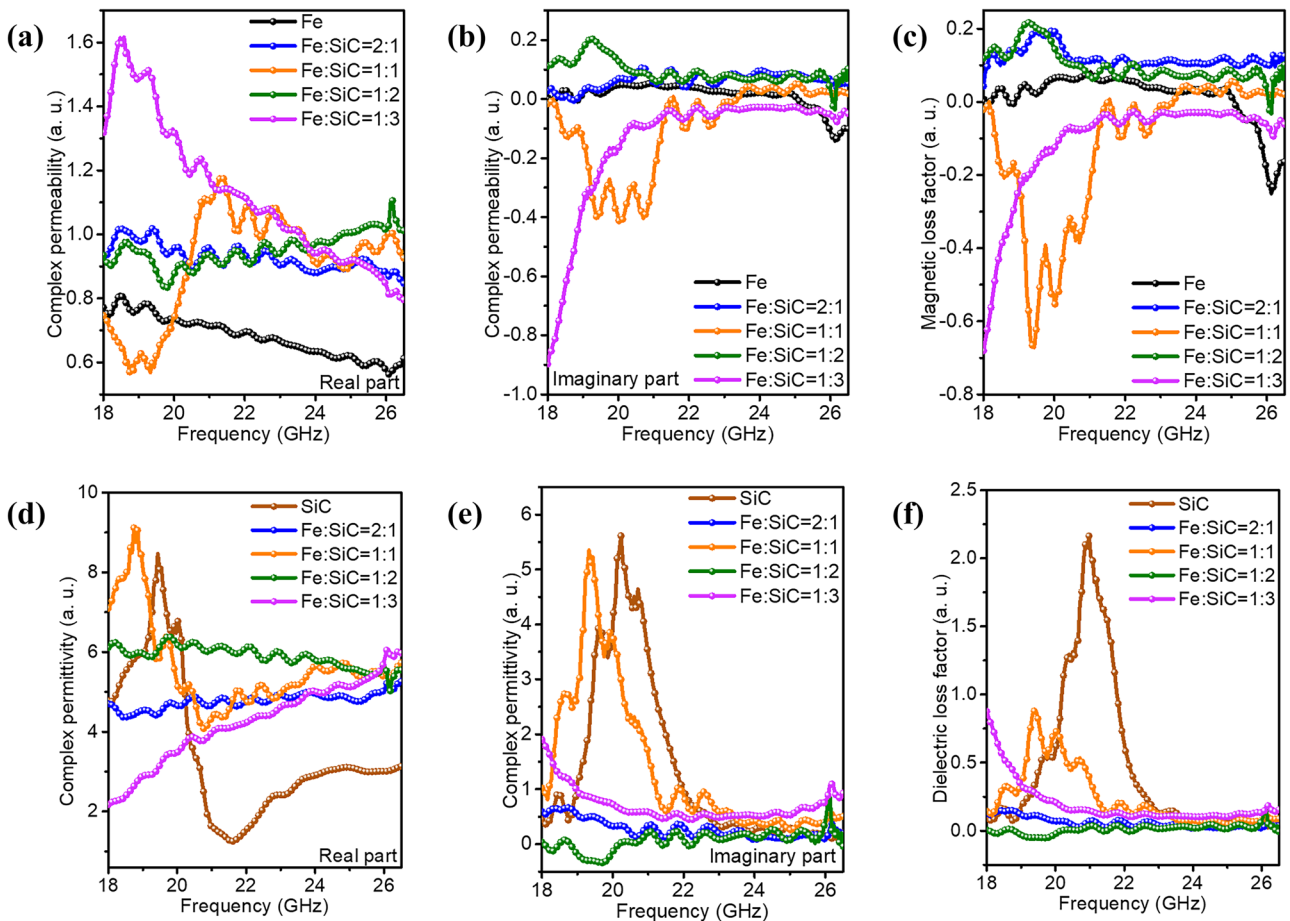


Fig. 4 Electromagnetic properties of Fe/SiC composites with different ratios of 2:1, 1:1, 1:2, and 1:3. **a** and **b** Relatively complex permeability. **c** The magnetic tangential loss. **d** and **e** Relatively complex permittivity. **f** The dielectric tangential loss

Figure 4d, e show the real part (ϵ') and imaginary part (ϵ'') of complex permittivity (ϵ_r) of SiC and Fe/SiC composites with different ratios. Except for the original SiC powders, the ϵ' and ϵ'' of Fe/SiC composite at the ratio of 1:1 had the highest values, reaching 9.2 and 5.4, respectively. In Fig. 4f, all the samples show a similar rising trend in $\tan\delta_e$, which becomes more obvious after coating SiC particles in the frequency region between 18 and 26.5 GHz. The values of $\tan\delta_e$ are above 0.5 for the samples with Fe to SiC of ratios of 1:1 and 1:3, and a clear peak is seen around 19 GHz. Especially, the values of $\tan\delta_e$ for the sample at ratios of 1:3 are the highest to 0.9 among all the samples. The values are particularly elevated in the frequency regions of 18 to 20 GHz, indicating the increased microwave energy loss abilities. Commonly, the improvement of dielectric loss capacity in gigahertz is always related to the polarization and relaxation process. Therefore, the Cole–Cole curves have been calculated and exhibited in Fig. 5; there are multiple polarization and relaxation processes that can be recognized in the core/shell structural Fe/SiC composites. Moreover, it can be noticed that the increased permittivity value is together with the decreased permeability value, indicating that an energy transformation phenomenon has occurred between the permittivity and permeability, which can be usually recognized in the closed-packed particle systems [53, 54]. Thus, the energy transformation results in increased dielectric loss performance and meanwhile induces the negative values of complex permeability.

After coating SiC, there is an insulating shell on the surface of the Fe particles, forming a large amount of Fe/SiC heterogeneous interface. Owing to different electrical conductivities between Fe and SiC powders, when the electromagnetic wave acts, the electric charge in the SiC powders could be transferred to the Fe powders by overcoming the barrier of the interface [55]. Meanwhile, the electric charge is accumulated at the interface, causing the induced charge to lag. Such an interfacial polarization behavior leads to polarization relaxation, which depletes more electromagnetic wave energy [56, 57].

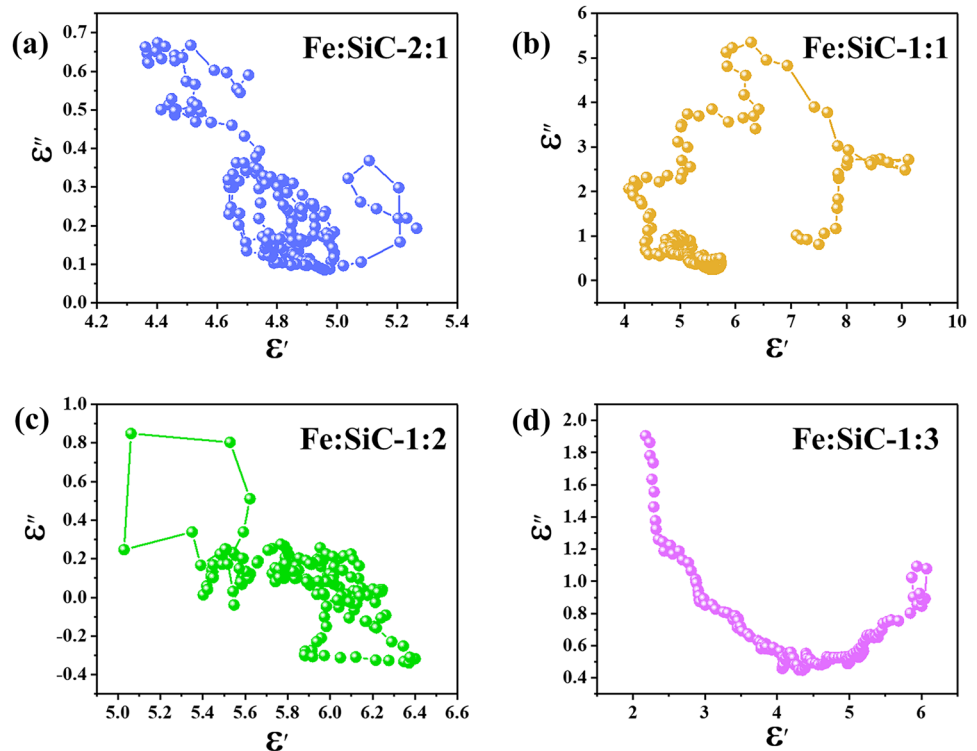
The EM absorption performance of Fe, SiC, and Fe/SiC composites was evaluated in the 18–26.5-GHz band by calculating the reflection loss (RL) according to transmission line theory [58]. The reflection loss RL (dB) could be described by the following equations [59]:

$$RL(\text{dB}) = 20 \lg \left| \frac{Z_{\text{in}} - 1}{Z_{\text{in}} + 1} \right| \quad (1)$$

$$Z_{\text{in}} = \sqrt{\frac{\mu_r}{\epsilon_r}} \tanh i \frac{2\pi f}{c} \sqrt{\mu_r \epsilon_r} d \quad (2)$$

As shown in Fig. 6a, b, Fe powders exhibited poor microwave absorption in the lower frequency range at 18–26.5 GHz. By incorporating dielectric SiC powders, the minimum reflection losses of Fe/SiC composites

Fig. 5 Cole–Cole curves of the core/shell structural Fe/SiC composites. The ratios of Fe and SiC are **a** 2:1, **b** 1:1, **c** 1:2, and **d** 1:3, respectively



with Fe:SiC = 2:1, 1:1, 1:2, and 1:3 were -25 dB at 20.7 GHz, -43 dB at 20.9 GHz, -24 dB at 18 GHz, and -51 dB at 19.4 GHz, respectively, as shown in

Fig. 6c–l. The mostly optimized Fe/SiC composite is at Fe to SiC ratio of 1:3, which is attributed to both improved dielectric loss and excellent impedance matching.

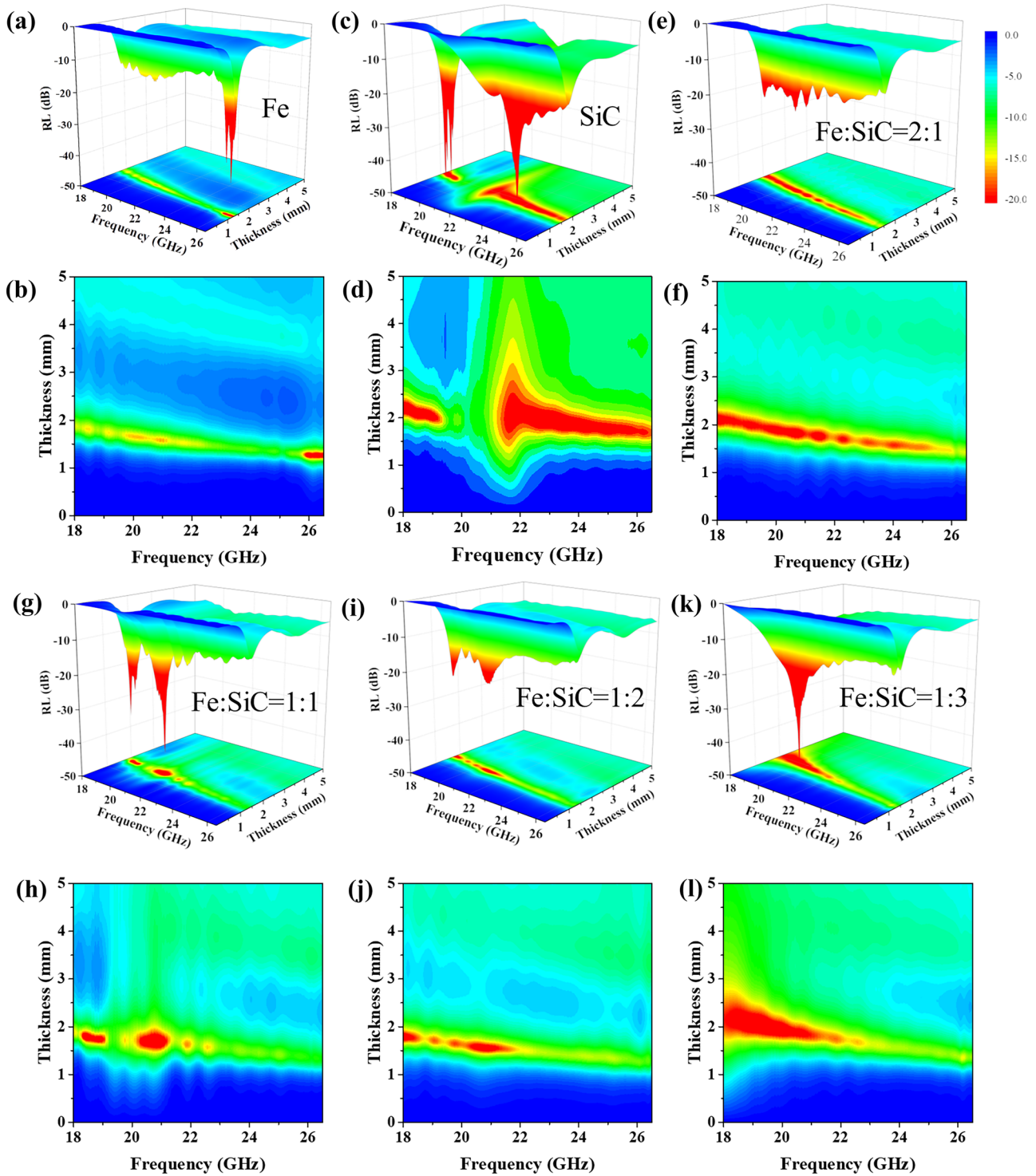


Fig. 6 The three-dimensional reflection loss mapping and corresponding contour plots. **a** and **b** Fe powders, **c** and **d** SiC powders, and Fe/SiC composites synthesized at ratios of Fe to SiC of **e** and **f**

g and **h** 1:1, **i** and **j** 1:2, and **k** and **l** 1:3. The thicknesses are ranging from 0 to 5 mm with an interval of 0.01 mm

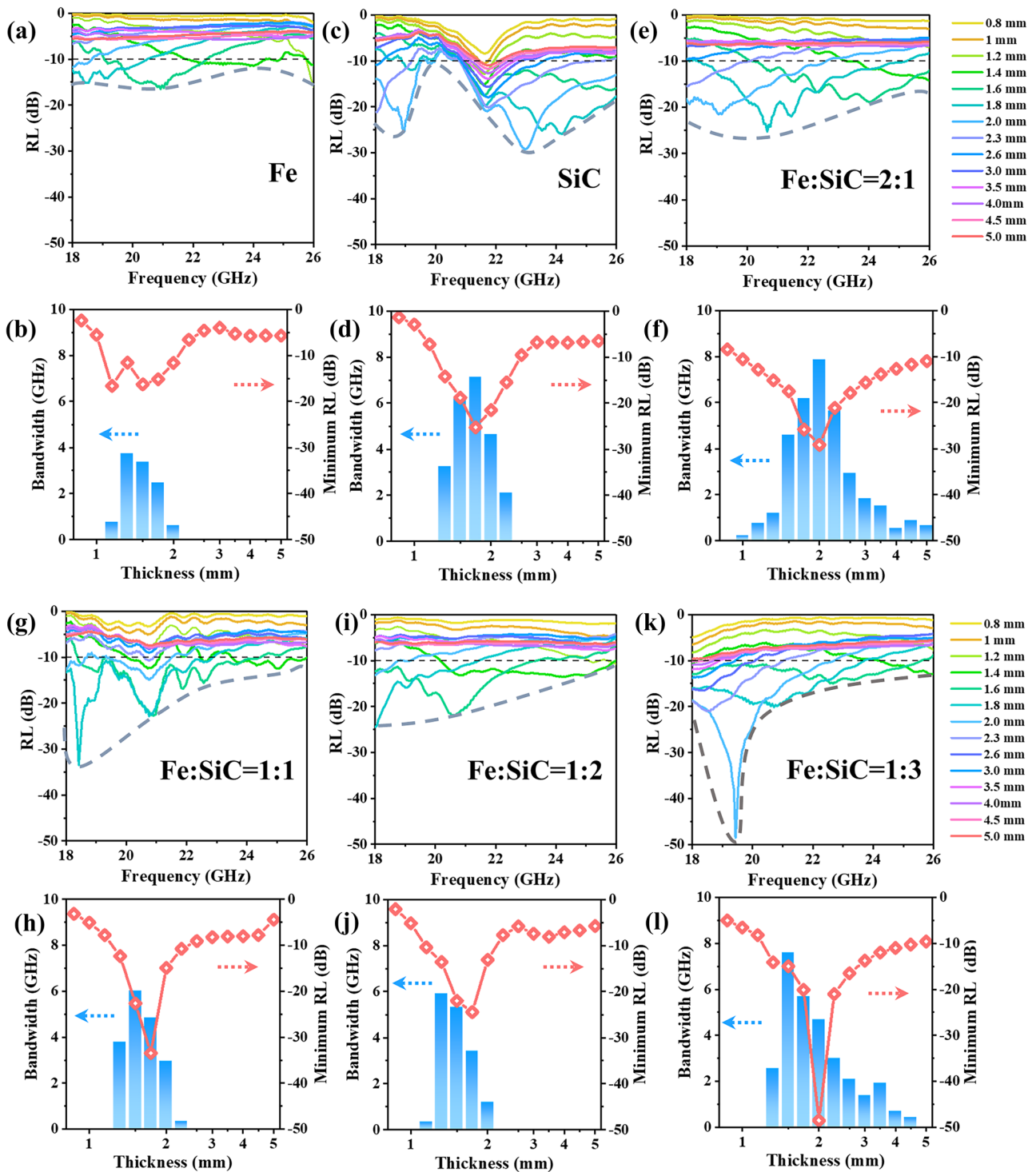


Fig. 7 Microwave absorbing performances of samples. **a** and **b** Fe powders, **c** and **d** SiC powders, and Fe/SiC composites synthesized at ratios of Fe to SiC of **e** and **f** 2:1, **g** and **h** 1:1, **i** and **j** 1:2, and **k** and **l** 1:3

Figure 7 provides the calculated reflection loss curves and bandwidth of Fe powders, SiC powders, and Fe/SiC composites. When the reflection loss is lower than -10 dB, it presents 90% absorption efficiency and

the corresponding frequency band is called the effective absorption bandwidth [60]. Figure 7a, b illustrate that the effective absorption bandwidth of original Fe powders was 3.3 GHz in the thickness range from 1.23

to 1.31 mm. In comparison, Fig. 7c–l indicate the effective absorption bandwidth of the Fe/SiC composites (Fe:SiC = 2:1, 1:1, 1:2, 1:3) centered at 20.9~26.5 GHz, 18.4~24.4 GHz, 18~23.3 GHz, and 18~25.6 GHz at the absorber thicknesses of 1.2~2.3 mm, 1.3~2.4 mm, 1.17~2.12 mm, and 1.2~4.69 mm, respectively. It is obvious that the introduced SiC shell broadened the effective absorption bandwidth. Meanwhile, higher SiC content caused a remarkable improvement in microwave absorption properties.

4 Conclusions

In conclusion, the Fe/SiC composites were synthesized by a heat-assisted surface adhesion process. By optimizing the component ratios of micro Fe and nano SiC powders, the relatively complex permittivity and permeability of composites could be effectively adjusted, in which the composites with a ratio of Fe to SiC of 1:3 present an improved electromagnetic impedance matching performance. For the best optimized Fe/SiC composite, the minimum reflection loss reached -51 dB at 19.4 GHz and the absorption bandwidth less than < -10 dB ranged from 18 to 25.6 GHz at the absorber thicknesses of 1.2–4.69 mm. This study provides a simple approach to synthesize the Fe/SiC composites for high-performance microwave absorption.

Funding Financial support was provided by Taif University Researchers Supporting Project number (TURSP-2020/135), Taif University, Taif, Saudi Arabia.

Declarations

Conflict of interest The authors declare no competing interests.

References

- Sun H, Che R, You X, Jiang Y, Yang Z, Deng J et al (2014) Cross-stacking aligned carbon-nanotube films to tune microwave absorption frequencies and increase absorption intensities. *Adv Mater* 26:8120–8125
- Chen H, Lu Z, Gao Q, Zuo Y, Liu X, Guo Z et al (2021) PVDF-Ni/PE-CNTs composite foams with Co-continuous structure for electromagnetic interference shielding and photo-electro-thermal properties. *Eng Sci* 16:331–340
- Wu N, Du W, Hu Q, Vupputuri S, Jiang Q (2021) Recent development in fabrication of Co nanostructures and their carbon nanocomposites for electromagnetic wave absorption. *Eng Sci* 13:11–23
- Zhao B, Deng J, Zhang R, Liang L, Fan B, Bai Z, Shao G, Park C et al (2018) Recent advances on the electromagnetic wave absorption properties of Ni based materials. *Eng Sci* 3:5–40
- Zhao B, Liang L, Bai Z, Gu X, Zhang R, Jiang Q et al (2021) Poly(vinylidene fluoride)/Cu@Ni anchored reduced-graphene oxide composite films with folding movement to boost microwave absorption properties. *Eng Sci* 14:79–86
- Li Y, Liao Y, Zhang J, Huang E, Ji L, Zhang Z et al (2021) High-entropy-alloy nanoparticles with enhanced interband transitions for efficient photothermal conversion. *Angew Chem Int Ed* 60:27113–27118
- Bahadur A, Saeed A, Iqbal S, Shoaib M, Ahmad I, Rahman M et al (2017) Morphological and magnetic properties of BaFe₁₂O₁₉ nanoferrite: a promising microwave absorbing material. *Ceram Int* 43:7346–7350
- Ying M, Zhao R, Hu X, Zhang Z, Liu W, Yu J et al (2022) Wrinkled titanium carbide (MXene) with surface charge polarizations through chemical etching for superior electromagnetic interference shielding. *Angew Chem Int Ed* 61:e202201323
- Liao Y, Li Y, Zhao R, Zhang J, Zhao L, Ji L et al (2022) High-entropy-alloy nanoparticles with ultra-mixed 21 elements for efficient photothermal conversion. *Natl Sci Rev*. <https://doi.org/10.1093/nsr/nwac041>
- Xie P, Liu Y, Feng M, Niu M, Liu C, Wu N, Sui K, Patil R, Pan D, Guo Z, Fan R et al (2021) Hierarchically porous Co/C nanocomposites for ultralight high-performance microwave absorption. *Adv Compos Hybrid Mater* 4:173–185
- Cheng W, Wang Y, Ge S, Ding X, Cui Z, Shao Q et al (2021) One-step microwave hydrothermal preparation of Cd/Zr-bimetallic metal-organic frameworks for enhanced photochemical properties. *Adv Compos Hybrid Mater* 4:150–161
- Zhang X, Liu Y, Qin G (2015) Break Snoek limit via superparamagnetic coupling in Fe₃O₄/silica multiple-core/shell nanoparticles. *Appl Phys Lett* 106:033105
- Zhang X, Li Y, Liu R, Rao Y, Rong H, Qin G (2016) High-magnetization FeCo nanochains with ultrathin interfacial gaps for broadband electromagnetic wave absorption at gigahertz. *ACS Appl Mater Inter* 8:3494–3498
- Liang B, Wang S, Kuang D, Hou L, Yu B, Lin L et al (2018) Facile synthesis and excellent microwave absorption properties of FeCo-C core-shell nanoparticles. *Nanotechnology* 29:085604
- Zhu Z, Sun X, Sun G, Xue H, Guo H, Fan X et al (2015) Microwave-assisted synthesis of graphene-Ni composites with enhanced microwave absorption properties in Ku-band. *J Magn Magn Mater* 377:95–103
- Sang G, Xu P, Yan T, Murugadoss V, Naik N, Ding Y et al (2021) Interface engineered microcellular magnetic conductive polyurethane nanocomposite foams for electromagnetic interference shielding. *Nano Micro Lett* 13:153
- Zhang X, Dong X, Huang H, Liu Y, Wang W, Zhu X et al (2006) Microwave absorption properties of the carbon-coated nickel nanocapsules. *Appl Phys Lett* 89:1679–1083
- Gao S, Zhao X, Fu Q, Zhang T, Zhu J, Hou F et al (2022) 1.Highly transmitted silver nanowires-SWCNTs conductive flexible film by nested density structure and aluminum-doped zinc oxide capping layer for flexible amorphous silicon solar cells. *J Mater Sci Technol* 126:152–160
- Khani O, Shoushtari MZ, Jazirehpour M, Sharms MH (2016) Effect of carbon shell thickness on the microwave absorption of magnetite-carbon core-shell nanoparticles. *Ceram Int* 42:14548–14556
- Zhang D, Xu F, Lin J, Yang Z, Zhang M (2014) Electromagnetic characteristics and microwave absorption properties of carbon-encapsulated cobalt nanoparticles in 2–18 GHz frequency range. *Carbon* 80:103–111
- Du Y, Liu W, Qiang R, Wang Y, Han X, Ma J et al (2014) Shell thickness-dependent microwave absorption of core-shell Fe₃O₄@C composites. *ACS Appl Mater Inter* 6:12997–13006
- Zhang T, Huang D, Yang Y, Kang F, Gu J (2013) Fe₃O₄/carbon composite nanofiber absorber with enhanced microwave absorption performance. *Mat Sci Eng B* 178:1–9

23. Qiao M, Lei X, Ma Y, Tian L, He X, Su K et al (2018) Application of yolk-shell Fe₃O₄@N-doped carbon nanochains as highly effective microwave-absorption material. *Nano Res* 11:1500–1519
24. Li N, Huang G, Li Y, Xiao H, Feng Q, Hu N et al (2017) Enhanced microwave absorption performance of coated carbon nanotubes by optimizing the Fe₃O₄ nanocoating structure. *ACS Appl Mater Inter* 9:2973–2983
25. Zhu L, Zeng X, Li X, Yang B, Yu R (2017) Hydrothermal synthesis of magnetic Fe₃O₄/graphene composites with good electromagnetic microwave absorbing performances. *J Magn Magn Mater* 426:114–120
26. Zhang X, Huang H, Dong X (2013) Core/shell metal/heterogeneous oxide nanocapsules: the empirical formation law and tunable electromagnetic losses. *J Phys Chem C* 117:8563–8569
27. Tian Y, Yang X, Nautiyal A, Zheng Y, Guo Q, Luo J, Zhang X et al (2019) One-step microwave synthesis of MoS₂/MoO₃@graphite nanocomposite as an excellent electrode material for supercapacitors. *Adv Compos Hybrid Mater* 2:151–161
28. Wang J, Wang Z, Liu R, Li Y, Zhao X, Zhang X (2017) Heterogeneous interfacial polarization in Fe@ZnO nanocomposites induces high-frequency microwave absorption. *Mater Lett* 209:276–279
29. Zhao B, Guo X, Zhao W, Deng J, Fan B, Shao G et al (2017) Facile synthesis of yolk-shell Ni@void@SnO₂(Ni₃Sn₂) ternary composites via galvanic replacement/Kirkendall effect and their enhanced microwave absorption properties. *Nano Res* 10:331–343
30. Su X, Jia Y, Wang J, Xu J, He X, Fu C et al (2013) Preparation and microwave absorption properties of Fe-doped SiC powder obtained by combustion synthesis. *Ceram Int* 39:3651–3656
31. Qi G, Liu Y, Chen L, Xie P, Pan D, Shi Z, Quan B, Zhong Y, Liu C, Fan R, Guo Z et al (2021) Lightweight Fe₃C@Fe/C nanocomposites derived from wasted cornstalks with high-efficiency microwave absorption and ultrathin thickness. *Adv Compos Hybrid Mater* 4:1226–1238
32. Xie P, Zhang Z, Wang Z, Sun K, Fan R et al (2019) Targeted double negative properties in silver/silica random metamaterials by precise control of microstructures. *Research* 1021368
33. Ji L, Zhao R, Hu X, Hu C, Shen X, Liu X et al (2022) Reconfigurable ferromagnetic resonances by engineering inhomogeneous magnetic textures in artificial magnonic crystals. *Adv Funct Mater* 2112956
34. Zhao L, He J, Li W, Liu X, Zhang J, Wen L et al (2021) Understanding the role of element grain boundary diffusion mechanism in Nd-Fe-B magnets. *Adv Funct Mater* 32:2109529
35. Zhang Z, Shi Z, Fan R, Guo M, Guo J, Qi X (2011) Microwave absorption properties of Fe@Al₂O₃ nanoembedments prepared by mechanosynthesis. *Mater Chem Phys* 130:615–618
36. Pan D, Yang G, Abo-Dief MH, Dong J, Su F, Liu C et al (2022) Vertically aligned silicon carbide nanowires/boron nitride cellulose aerogel networks enhanced thermal conductivity and electromagnetic absorbing of epoxy composites. *Nano-Micro Lett* 14:118
37. Yao F, Xie W, Yang M, Zhang H, Gu H, Du A et al (2021) Interfacial polymerized copolymers of aniline and phenylenediamine with tunable magnetoresistance and negative permittivity. *Mater Today Phys* 21:100502
38. Yan L, Wang J, Han X, Ren Y, Liu Q, Li F (2010) Enhanced microwave absorption of Fe nanoflakes after coating with SiO₂ nanoshell. *Nanotechnology* 21:095708
39. Li Y, Cheng H, Wang N, Zhou S, Xie D, Li T (2019) Annealing effects on the microstructure, magnetism and microwave-absorption properties of Fe/TiO₂ nanocomposites. *J Magn Magn Mater* 471:346–354
40. Zhang W, Bie S, Chen H, Lu Y, Jiang J (2014) Electromagnetic and microwave absorption properties of carbonyl iron/MnO₂ composite. *J Magn Magn Mater* 358:1–4
41. Lin H, Zhu H, Guo H, Yu L (2007) Investigation of the microwave-absorbing properties of Fe-filled carbon nanotubes. *Mater Lett* 61:3547–3550
42. Kuang J, Jiang P, Liu W, Cao W (2015) Synergistic effect of Fe-doping and stacking faults on the dielectric permittivity and microwave absorption properties of SiC whiskers. *Appl Phys Lett* 106:212903
43. Liu X, Zhang D, Zhao R, Zhang Y, Zhang M, Wang J et al (2018) Tuning microwave absorption properties by hybridizing heterogeneous components for core@shell structural Fe@SiC flakes. *J Magn Magn Mater* 462:46–52
44. Deng L, Wang X, Hua X, Lu S, Wang J, Wang H et al (2022) Purification of β-SiC powders by heat treatment in vacuum. *Adv Compos Hybrid Mater* 5:431–437
45. Hou Y, Cheng L, Zhang Y, Yang Y, Deng C, Yang Z et al (2017) Electrospinning of Fe/SiC hybrid fibers for highly efficient microwave absorption. *ACS Appl Mater Interfaces* 9:7265–7271
46. Zhou P, Chen J, Liu M, Jiang P, Li B, Hou X (2017) Microwave absorption properties of SiC@SiO₂@Fe₃O₄ hybrids in the 2–18 GHz range. *Int J Miner Metall Mater* 24:804–813
47. Liu Y, Liu X, Wang X, Wu W (2014) Electromagnetic and microwave absorption properties of Fe coating on SiC with metal organic chemical vapor reaction. *Chinese Phys Lett* 31:047702
48. Chang X, Chen L, Chen J, Zhu Y, Guo Z (2021) Advances in transparent and stretchable strain sensors. *Adv Compos Hybrid Mater* 4:435–450
49. Pan D, Dong J, Yang G, Su F, Chang B, Liu C et al (2022) Ice template method assists in obtaining carbonized cellulose/boron nitride aerogel with 3D spatial network structure to enhance the thermal conductivity and flame retardancy of epoxy-based composites. *Adv Compos Hybrid Mater* 5:58–70
50. Zhu Q, Huang Y, Li Y, Zhou M, Xu S, Liu X et al (2021) Aluminum dihydric tripolyphosphate/polypyrrole-functionalized graphene oxide waterborne epoxy composite coatings for impermeability and corrosion protection performance of metals. *Adv Compos Hybrid Mater* 4:780–792
51. Jiang N, Hu D, Xu Y, Chen J, Chang X, Zhu Y et al (2021) Ionic liquid enabled flexible transparent polydimethylsiloxane sensors for both strain and temperature sensing. *Adv Compos Hybrid Mater* 4:574–583
52. He J, Wang X, Zhang Y, Cao M (2016) Small magnetic nanoparticles decorating reduced graphene oxides to tune the electromagnetic attenuation capacity. *J Mater Chem C* 4:7130–7140
53. Wu H, Zhong Y, Tang Y, Huang Y, Liu G, Sun W, Xie P, Pan D, Liu C, Guo Z et al (2022) Precise regulation of weakly negative permittivity in CaCu₃Ti₄O₁₂ metamaterials by synergistic effects of carbon nanotubes and graphene. *Adv Compos Hybrid Mater* 5:419–430
54. Wu H, Sun H, Han F, Xie P, Zhong Y, Quan B, Zhao Y, Liu C, Fan R, Guo Z et al (2022) Negative permittivity behavior in flexible carbon nanofibers-polydimethylsiloxane films. *Eng Sci* 17:113–120
55. Yang H, Cao W, Zhang D, Su T, Shi H, Wang W et al (2015) NiO hierarchical nanorings on SiC: enhancing relaxation to tune microwave absorption at elevated temperature. *ACS Appl Mater Interfaces* 7:7073–7077
56. Bowler N (2006) Designing dielectric loss at microwave frequencies using multi-layered filler particles in a composite. *IEEE Trans Dielectr Electr Insul* 13:703–711
57. Guo J, Li X, Chen Z, Zhu J, Mai X, Wei R et al (2022) Magnetic NiFe₂O₄/polypyrrole nanocomposites with enhanced electromagnetic wave absorption. *J Mater Sci Technol* 108:64–72
58. Li Y, Liao Y, Ji L, Hu C, Zhang Z, Zhang Z et al (2022) Quinary high-entropy-alloy@graphite nanocapsules with tunable interfacial impedance matching for optimizing microwave absorption. *Small* 18:2107265
59. Wen B, Cao M, Lu M, Cao W, Shi H, Liu J et al (2014) Reduced graphene oxides: light-weight and high-efficiency electromagnetic interference shielding at elevated temperatures. *Adv Mater* 26:3484–3489

60. Zhang Y, Huang Y, Zhang T, Chang H, Xiao P, Chen H et al (2015) Broadband and tunable high-performance microwave absorption of an ultralight and highly compressible graphene foam. *Adv Mater* 27:2049–2053

Publisher's Note Springer Nature remains neutral with regard to jurisdictional claims in published maps and institutional affiliations.